Characterization of the Near-Plume Region of a Laboratory BaO Hollow Cathode Operating on Xenon and Iodine Propellants

IEPC-2017-465

Presented at the 35th International Electric Propulsion Conference
Georgia Institute of Technology • Atlanta, Georgia • USA
October 8 – 12, 2017

Zachary R. Taillefer[1] and John J. Blandino[2]
Worcester Polytechnic Institute, Worcester, MA, 01609

James Szabo[3]
Busek Co. Inc., Natick, MA, 01760

Abstract: A low power (< 5 A), BaO hollow cathode was operated on xenon and iodine propellants. Its discharge current and voltage, and plume properties are reported for xenon and iodine with the cathode at similar operating conditions for each. The overall performance of the BaO cathode on iodine was comparable to xenon. The cathode operating on iodine required slightly higher power for ignition and discharge maintenance compared to xenon, as evident by the higher keeper and anode potentials. Plasma properties in the near-plume region were measured using an emissive probe and single Langmuir probe. For both propellants, the plasma density, electron energy distribution function (EEDF), electron temperature, select reaction rate coefficients and time-resolved plasma potentials are reported. For both propellants the cathode operated the same keeper (0.25 A) and discharge current (3.1 A), but the keeper and anode potentials were higher with iodine; 27 V and 51 V for xenon, and 30 V and 65 V for iodine, respectively. For xenon, the mean electron energy and electron temperature were 7.5 eV and 0.7 eV, with bulk drift energy of 6.6 eV. For iodine, the mean electron energy and electron temperature were 6.3 eV and 1.3 eV, with bulk 4.2 eV. A literature review of relevant collisional processes and associated cross sections for an iodine plasma is also presented.

Nomenclature

A	=	amplitude of ac signal
A_p	=	probe surface area
e	=	elementary charge
ε	=	energy
ε_d	=	electron drift energy
f	=	distribution function
H	=	normalization constant
Γ	=	particle flux
I	=	current
I_A	=	anode current
I_K	=	keeper current

[1] PhD Candidate, Aerospace Engineering Program, Mechanical Engineering Department, ztaillefer@wpi.edu.
[2] Associate Professor, Aerospace Engineering Program, Mechanical Engineering Department, blandino@wpi.edu.
[3] Chief Scientist, Hall Thruster Group, jszabo@busek.com.

I_{sp} = specific impulse
k_b = Boltzmann's constant
m_e = electron mass
m_i = ion mass
P_{pot} = iodine reservoir pressure
ϕ_f = floating potential
ϕ_p = plasma potential
Q = volumetric flow rate
σ = cross section
T_e = electron temperature
T_{Pot} = iodine reservoir temperature
v_e = electron velocity
V = potential
V_K = keeper potential
V_A = anode potential

I. Introduction

HOLLOW cathodes have been the standard electron source for ion and Hall effect thrusters for decades. A typical hollow cathode consists of a low work function emitter, tube to house the emitter, restricting orifice, resistive heating element and keeper electrode. The low work function emitter readily emits electrons when heated to sufficient temperature. The cathode tube provides an orifice that restricts the propellant flow and maintains a static pressure on the order of a torr to tens of torr (1-50 Torr) [4]. A plasma is generated upstream of the restricting orifice at the emitter, which keeps the emitter at emission temperatures and allows the heating element to be turned off. The keeper electrode extracts electrons from the internal plasma to be used for thruster discharge plasma generation and maintenance, and to neutralize the ion beam. One common cathode emitter is a porous tungsten matrix impregnated with a mixture of barium, calcium and aluminum oxides. Low energy electrons are liberated from a barium-on-oxide monolayer on the surface of the porous tungsten through heating. The $BaO:CaO:Al_2O_3$ mixture provides the barium monolayer through chemical reactions. Typical compositions for the impregnant mixture include 4:1:1, 5:3:2 and 6:1:2, where the notation indicates the stoichiometric coefficient of $BaO:CaO:Al_2O_3$. Barium and barium oxide continuously evaporate from the emitter surface at emission temperatures, but are replenished at the surface by the impregnate. The replenishment requires two processes: generation of barium by a reaction with tungsten and diffusion of barium to the emitter surface.

Hollow cathodes typically operate on the same propellant as the companion thruster. The most common propellants for electrostatic thrusters have been noble gases, specifically xenon, with some exceptions such as mercury and cesium, during their early development [1]. Many other propellants have been investigated in the laboratory including krypton, argon and molecular gases (oxygen and nitrogen) [2, 3, 4]. Some condensable propellants have been tried including magnesium, zinc, bismuth and iodine [5, 6, 7]. Xenon is generally preferred to

Table 1: Physical properties of candidate propellants for electric thrusters [50].

Propellant	Mass (amu)	T_m (°C)	T_b (°C)	First Ionization Potential (eV)	Price ($/kg)*
Xenon	131.3	-111.79 (tp)	-108.12	12.13	1,138
Krypton	83.8	-157.38 (tp)	-153.22	14.00	295
Cesium	132.9	28.5	671	3.89	40,000
Mercury	200.6	-38.837 (tp)	356.73	10.44	4
Magnesium	24.3	650	1090	7.65	3
Zinc	65.4	419.53	907	9.39	0.5
Bismuth	209.0	271.40	1564	7.29	6
Iodine (I_2)	126.9	113.75	184.67	10.45 (9.35)	500
Nitrogen (N_2)	28.0	-210.0 (tp)	-195.8	15.58	3
Oxygen (O_2)	32.0	-218.8 (tp)	-183.0	12.07	3

*Typical commercial prices in 2017

other propellants options since it is inert, not hazardous to handle, does not condense on surfaces (above cryogenic temperatures), easy to ionize (low ionization energy), has a fairly large mass and can be easily stored at high pressure [1]. Although storing xenon at high pressure requires a thick-walled tank, a high-pressure tank is the simplest storage and feed system option in design and concept. Other propellant options considered may be preferable to xenon with respect to one or more of these categories, but have other disadvantages, making xenon the practical choice for most applications. Mercury and cesium have a large atomic mass and low ionization potentials but are highly reactive and hazardous to handle. All other noble (krypton, argon) and inert gases (nitrogen) are less expensive ($/kg) than xenon; however, they have a lower atomic (or molecular) mass, are harder to ionize than xenon and still require high pressure storage tanks. Condensable propellants, i.e. those that condense at "typical" laboratory or spacecraft feed system temperatures, have significant storage advantages, and in some cases, low ionization potentials and large (first) ionization cross sections. Some condensable propellants offer system-level benefits (high T/P or high I_{sp}) but can require significant heating (100's of degrees Celsius) to generate adequate vapor pressure. Iodine has a unique property (in terms of propellant candidates); it will sublimate at a relatively low temperature (~50° C). Iodine was first considered as a propellant in the early 2000's and is a candidate to replace xenon as the propellant for deep space missions requiring high throughput [8, 9]. Table 1 lists the physical properties of several candidate propellants for electric thrusters.

Xenon and iodine have first-ionization energies of 12.13 eV and 10.45 eV (9.35 eV for I_2), respectively. Both have similar ionization cross sections; however, for electron impact energies below ~100 eV the atomic iodine cross section is approximately 50% larger than xenon. Iodine is typically diatomic but has a relatively low dissociation energy (1.57 eV at 298 K) and will almost entirely dissociate at high temperature (>1000 K) [10]. The molecular iodine ionization cross section is twice as large as xenon for electron energies below ~100 eV and is larger than the xenon cross section for electron energies up to 500 eV. Figure 1 shows the ionization cross sections for iodine (I and I_2) and xenon for electron energies up to 500 eV. Iodine has shown similar performance characteristics to xenon in Hall thrusters [11]. In tests performed with a BHT-200 HET, Szabo *et al*. reported fractions of high-energy ion flux comprised of dimers (I_2^+) ranged between 3%-10% in the HET beam with low levels of doubly (1.5%) and triply (0.3%) charged iodine and xenon [7, 12].

In general, for typical EP-powered missions, assuming a fixed spacecraft dry mass, the mass (or change in mass) required for a particular Δv will not change with propellant (for a given I_{sp}), thus the required propellant mass will remain largely the same with xenon and iodine, which have demonstrated comparable specific impulse. Also, while the cost savings with iodine is significant for the fuel alone (approximately 50% reduction) the total cost of the propellant for a large mission is on the order of ~0.1% of the total mission cost [8]. For example, a typical GEO satellite carries approximately 100 kg of propellant, which for xenon would cost $100k-200k; however, the total spacecraft cost is approximately $100M [8]. Therefore, while the cost of propellant is a consideration, it may not be a driving factor for a deep-space/Flagship mission. The real mission systems benefit comes from the elimination of the high-pressure (thick-walled) propellant tank required for xenon. Many factors determine the mass of the propellant tank but reasonable estimates suggest gaseous propellant tank mass can be up to 35% of the total propellant mass [13]. Since iodine can be stored at low pressure (10's of torr) and higher density, the propellant tank can be a much smaller in terms of volume and mass. Iodine also lends itself to tanks made of non-traditional and light materials such as thermoplastics—further reducing the mass contribution of the propellant tank. The reduction in tank mass lowers the spacecraft dry mass, which in turn allows for additional propellant for a given wet mass; this is quite desirable since it effectively increases mission life for an equivalent launch wet mass and cost.

Since iodine can be stored as a solid at approximately three times the density of xenon, the overall tank size can be significantly reduced and conformal tanks can be considered. This would benefit spacecraft of all sizes, but it would benefit small, volume-starved spacecraft in particular, specifically ESPA-class (180 kg) and

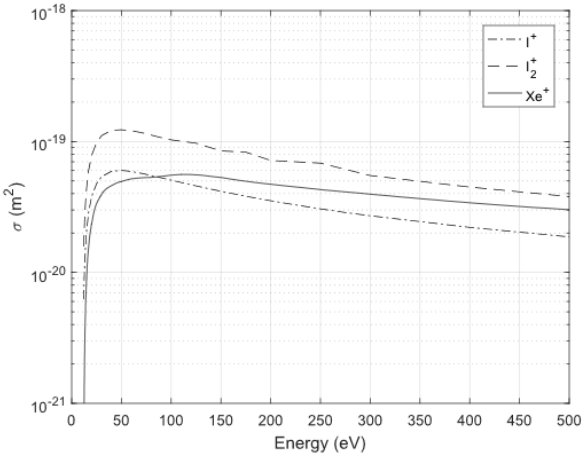

Figure 1. Ionization cross sections for iodine (I and I_2) [14] and xenon [15].

smaller. Small spacecraft often are secondary payloads and have fixed or prescribed platforms and buses. A smaller propellant tank would allow for the equivalent (or more) propellant to be stored compared to xenon, but allow more physical space for the payload, instrumentation, for the same spacecraft mass (i.e. launch cost). As mentioned above, iodine is also stored at low pressure, approximately 1000 times lower than xenon. This is a system-level benefit when spacecraft are being considered as secondary payloads as the main payload takes priority and a high-pressure vessel in the secondary payload would be considered a risk.

Iodine has at least one major hurdle to overcome before it can be considered as a replacement for xenon for all missions—its effectiveness and long-term durability have not yet been demonstrated when used as the working gas for plasma-discharge based electron sources, i.e. hollow cathodes. For high-power/high-throughput missions a "bi-propellant" system may be considered where the cathode operates on xenon and the thruster on iodine; however, even for large systems this is not ideal and for small, volume- and power-starved spacecraft it may nullify some of the benefits of using iodine propellant. Iodine propellant has been demonstrated with an electride (C12A7) cathode for approximately 50 hours [14]. Electride is still in the development stage and far from a replacement for BaO or LaB_6 emitters in hollow cathodes as more testing is required (i.e. duration testing). Iodine is also known to react with typical cathode materials including stainless steel and tantalum [15]. A flight demonstration of a HET and cathode operating on iodine on a 12U spacecraft was approved in 2015 by NASA's Space Technology Mission Directorate (STMD). This spacecraft, known as iSat and is being co-developed by NASA Glenn Research Center (GRC) [16], Marshall Space Flight Center (MSFC) [17] and Busek Co. Inc. and is scheduled for launch in 2018. Busek Co. Inc. demonstrated more than 100 cathode cycles and 50 hours of operation with a laboratory model BaO hollow cathode, yet the cathode remains a key area of risk for the iSat system [18]. Demonstrating operation with iodine in conjunction with a proven emitter material with flight heritage is critical to iodine being considered a replacement for xenon as an electrostatic thruster propellant. The work described in this paper was undertaken in order to characterize a BaO hollow cathode operating on iodine and compare the performance to a known propellant, xenon.

This paper is organized as follows. In Section II, the experimental setup is described, including a description of the facility, hollow cathode and propellant feed systems. Section III outlines the diagnostic methods and apparatus used to characterize the cathode plume, and includes a literature review of cross sections for known iodine reactions. The results are presented in Section IV and discussion follows in Section V.

II. Experimental Setup

Testing was conducted at Busek Co. Inc. in the T-1 test facility, which is a stainless steel cylindrical tank with a 6-foot diameter and length of 4 ft. High vacuum pumping is provided by a 16-inch diffusion pump and single stage cryogenic pump, shrouded by liquid nitrogen (LN2) panels. The T-1 vacuum chamber can achieve a base pressure of $5.0 \cdot 10^{-6}$ torr and a pumping speed of approximately 80,000 l/s on xenon. The LN2 panels aid in pumping, but are primarily used to condense iodine and prevent contamination of the cryogenic panel and other vacuum equipment from iodine.

The hollow cathode used in this study was a laboratory version of the BHC-2500, termed the Modular Hollow Cathode (MHC) due to its configurability. The MHC is shown in Figure 2. The cathode tube, heater and keeper could be easily modified, removed and replaced in the event of a failure or to try different configurations. The MHC consisted of a molybdenum-rhenium cathode tube with tungsten orifice plate with 1.0 mm diameter orifice. A swaged Ta-Ta heater wire with MgO insulation was used to bring the BaO-W emitter to emission temperature. The keeper was a graphite plate with 2.5 mm orifice with approximately 1.0 mm gap between keeper and cathode tube. The keeper was held in place by a threaded rod and alumina tube, seated in a Swagelok™ bulkhead. The threaded rod also provided power to the keeper and the alumina tube offered electrical insulation to prevent stray arcing. The heater electrical connection was a custom clamp isolated from ground using boron-nitride isolators.

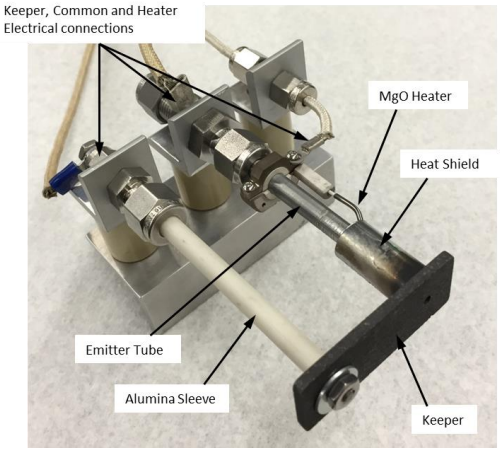

Figure 2. MHC used for xenon and iodine comparison testing.

The MHC was operated in triode mode, where the keeper is energized and the cathode discharged to an anode, with cathode common grounded to facility ground. A graphite flat plate with 1.3 cm through hole was used as the anode. The hole prevented iodine contamination and buildup on the anode plate, and allowed Langmuir probe access to the near-keeper region of the cathode plume along the cathode centerline.

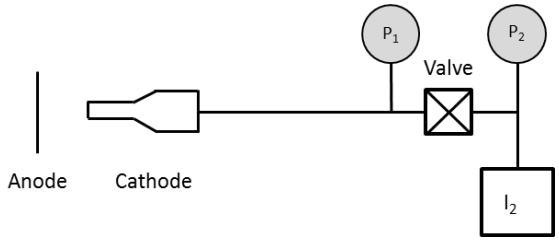

Figure 3. Schematic of the iodine feed system and cathode.

Two separate feed systems were used, one for each propellant type. High purity, propulsion-grade xenon (99.999+) xenon was feed to the MHC from a gas bottle outside the vacuum chamber. The xenon flow rate was measured and regulated by an MKS 1179 mass flow controller. Pure molecular iodine (99.995+) was supplied using a custom iodine feed system, which consisted of an iodine reservoir, iodine resistant feed lines, isolation solenoid valve and temperature compensated pressure sensors (0-5 psia). Figure 3 shows a schematic of the iodine feed system and cathode. The pressure on either side of the valve was monitored by two of the Omega pressure sensors. The pressure measurements were used to crudely estimate flow rate, monitor the iodine reservoir pressure and troubleshoot clogs in the feed system. The temperature in the iodine reservoir and propellant lines were independently controlled by Omega temperature controllers using thermocouples and ribbon heaters. The entire feed system was wrapped in high temperature insulation to minimize the possibility of cold spots. Clogs could be generated by pure iodine in a cold spot or iodine compounds formed from various reactions at elevated temperatures. To this end, the propellant feed lines were kept at a much higher temperature than the iodine reservoir, approximately 50°C above the reservoir temperature.

III. Diagnostics

This section describes the diagnostic methods and devices used to interrogate the cathode plume plasma in the near-keeper region. Emissive and Langmuir probes were used to measure the plasma potential and plasma properties. The emissive probe measured the time-resolved plasma potential with a bandwidth of 1 MHz. The Langmuir probe was used to calculate plasma properties including the plasma density and electron energy distribution function (EEDF). The EEDF was then used with known cross sections to calculate reaction rate coefficients for collisional process in the plasma.

A. Emissive Probe

A floating emissive probe can provide a direct measurement of the floating potential using a thermionically emitting filament immersed in the plasma [19]. In this technique, an electrically isolated, emitting wire is used to provide a direct measurement the floating potential, that for a strongly emitting probe is approximately equal to the plasma potential. The floating point technique is the most widely used emissive probe method due to the ease of implementation and broad range of applicability in a variety of plasma conditions [20]. Typically, a loop of tungsten wire is heated to emission temperatures by passing a current through it. For the floating point method, the entire measurement circuit is isolated from facility ground and floats very close to the plasma potential.

For a non-emitting planar surface, both ions and electrons are collected, and a sheath will develop. For an emitting surface, the inclusion of an additional flux term is necessitated by the emitted electrons. As the temperature of the surface is increased, the flux of emitted electrons increases. This additional flux will change the floating potential of the surface through the sheath structure. The potential difference between the floating potential and plasma potential is given by

$$\Delta V = -\left(\frac{T_e}{e}\right)\ln\left(\frac{1-\Gamma}{\sqrt{2\pi m_e/m_i}}\right) \tag{1}$$

where Γ is the ratio of emitted and collected electron flux [20]. As the emission current is increased, the floating potential reaches a value close to the plasma potential (within an electron temperature, T_e/e). This critical flux, where the difference between the floating potential and local plasma potential is a minimum, or the point at which floating potential "saturates", is given by

$$\Gamma = 1 - 8.3\sqrt{\frac{m_e}{m_i}} \tag{2}$$

This critical flux represents a space-charge-limited emission current and reduces the difference between the floating potential and plasma potential to the order of the electron temperature ($\Delta V \approx -T_e/e$). More rigorous analysis, which includes the sheath [21] and pre-sheath [22] at critical emission shows the difference between the floating potential and plasma potential is approximately twice the electron temperature.

$$\Delta V \approx -1.8\frac{T_e}{e} \tag{3}$$

A corresponding rigorous solution has not been established for the case of cylindrical geometry for the emitting surface, but the phenomenon is the same; as the electron emission increases the floating potential rises and reaches a value near the plasma potential. For the cylindrical geometry the sheath conditions have been considered in the saturation condition [23]. If the probe floating potential is lower than the local plasma potential, the probe surface will repel the emitted electrons and this electron current will appear in the measurement circuit as ion current to the probe. When the potential of the probe is positive relative to the local plasma potential, emitted electrons will be collected by the probe, leaving the collected electron current unaffected. The electron emission cannot be increased arbitrarily due to a space-charge limitation around the probe. In this case a double sheath will form around the probe and the slow-moving electrons emitted by the probe will be reflected back to the surface. The floating emissive probe with cylindrical geometry still provides a direct measurement of the plasma potential within $1\,T_e/e$ [24].

The floating point method is capable of following fast temporal fluctuations in plasma potential in the low RF regime. The main limitation of the frequency response of the probe is its own stray capacitance generated by the fluctuating plasma potential in the vicinity of probe surface [19]. It is possible to overcome significant errors due to stray capacitance by using a high impedance between the probe tip and measurement circuitry. When the probe emission is sufficient such that the floating potential is on the order of the electron temperature as described above, temporal measurements of the plasma potential can be performed. This is a distinct advantage of using an emissive probe and the floating point method.

When coupled with a high impedance, high bandwidth measurement circuit it can follow a rapidly (frequency > 500 kHz) changing plasma potential. The emissive probe used in this experiment consisted of an electrically isolated, floating loop of 0.0762 mm diameter tungsten wire. A custom measurement circuit allowed the plasma potential to be monitored by an oscilloscope and collected using a custom LabVIEW VI and GPIB interface. A DC power supply, isolated from facility ground, sourced the current necessary to heat the filament to emission temperature.

The emissive probe was located approximately 7 mm downstream of the keeper exit plane, along the center axis of the cathode. The top of the emissive probe loop was 1-2 mm below the cathode centerline, to allow the moving Langmuir probe to traverse the near-plume region without damaging the emissive probe.

B. Single Langmuir Probe

A single, cylindrical Langmuir probe (SLP) was used to measure the plasma density and EEDF in the cathode plume. The probe voltage is measured directly using a simple voltage divider and unity gain buffer. The probe current was simultaneously measured using a small shunt resistor and differential amplifier. A two stage, four pole low pass Butterworth filter was used to filter noise on the current measuring branch of the circuit.

The probe must be sufficiently small as to not disturb the surrounding plasma being interrogated but not so small that the collected current is not measureable. The SLP used for this experiment consisted of a 0.076 mm x 4 mm (0.003 in x 0.079 in) high purity tungsten wire (probe tip), supported and insulated by 0.70 mm OD x 0.50 mm ID x 7.0 mm L (0.028 in OD x 0.020 in ID x 0.276 in L) borosilicate tube (probe holder). The borosilicate tube was supported and insulated by a 6.35 mm OD x 4.78 mm ID (0.25 in OD x 0.188 in ID) alumina tube (approximately 300 mm in length) fixed at one end in a Swagelok™ tee. The end of the borosilicate tube was sealed with 904 Zirconia paste. The interface between the borosilicate tube and the alumina was also sealed with 904 Zirconia paste to hold the borosilicate tube in place and prevent plasma penetration. To securely seat the alumina tubing in the reducing union without the risk of

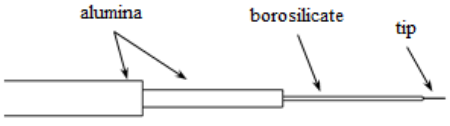

Figure 4. SLP tip schematic.

fracture, Teflon ferrules were used in place of stainless steel (this method also does not require any modifications to the Swagelok™ union).

The probe position relative to the cathode was controlled by two, stacked PI miCos VT-80 linear translation stages, providing two-axis control in the horizontal plane (300 mm range in x-direction and 200 mm range in y-direction). Each translation stage was powered by a "2phase-042" stepper motor with an SMC Pullox motor-control module, and equipped with full-step encoders and integrated limit switches. The stepper motors offered a maximum translation speed of 13 mm/sec and a knowledge resolution of 5 microns. Communication with the motor occurs through two RS 232 DB-9 cables providing independent power and data, with a PI miCos supplied LabVIEW virtual instrument (VI) as the control interface. The VI allowed independent control of each stage, with the capability of specifying absolute or relative probe displacement. Prior to each test, the acceptable probe translation area was mapped to ensure unobstructed probe translations.

There was a concern that iodine would condense on the probe tip, and that this contamination would inhibit current collection, particularly in the exponential region of the IV curve. A reduction in collected current in this region of the IV curve would result in an artificially lowered measured electron temperature and an inaccurate EEDF. To mitigate iodine condensation on the probe tip, during each voltage sweep the probe voltage was driven well into (10-20 V) the electron saturation region to heat the probe tip and evaporate any condensed iodine. This procedure did not affect the IV curve, subsequent analysis, or generate any hysteresis.

C. Second Harmonic Method

The Druyvesteyn method [25] is based on the fact that the EEDF is proportional to the second derivative of the probe current with respect to probe voltage. Equation 4 relates the second derivative of the probe characteristic below the plasma potential to the non-normalized EEDF. Even with low-noise circuitry and low-pass filtering the I-V curve has white noise. This noise is amplified by each numerical differentiation. As a result, noise amplification is unavoidable using numerical differentiation and will propagate to the distribution function. At best this will increase the uncertainty of the electron temperature; at worst it can make the distribution function non-physical (i.e. negative probabilities).

$$F(\varepsilon) = \frac{4}{e^2 A_p}\left(\frac{mV}{2e}\right)^{1/2}\frac{d^2I}{dV^2} \tag{4}$$

To reduce noise, a widely used method to determine the second derivative of a Langmuir probe trace uses a small amplitude (relative to the expected electron temperature), high frequency (1-100kHz) signal superimposed over the probe bias [26, 27, 28, 29, 30]. This signal is commonly referred to as the "AC signal" and that terminology has been adopted for this work. With the ac signal superimposed over the ramping probe voltage, the probe current then becomes $I = I(V + A\sin\omega t)$. It can be shown, using a Taylor series expansion, that the second derivative of the probe current is proportional to the amplitude of the second harmonic term in the expansion (last bracketed term in Eq. (5) [30].

$$\begin{aligned} I(V) = {} & I(V) + \frac{A^2}{4}\frac{d^2I(V)}{dV^2} + \frac{A^4}{64}\frac{d^4I(V)}{dV^4} + \cdots \\ & + \left[A\frac{dI(V)}{dV} + \frac{A^3}{8}\frac{d^3I(V)}{dV^3} + \cdots\right]\sin\omega t + \cdots \\ & - \left[\frac{A^2}{4}\frac{d^2I(V)}{dV^2} + \frac{A^4}{48}\frac{d^4I(V)}{dV^4} + \cdots\right]\cos 2\omega t + \cdots \\ & + \text{higher order terms} \end{aligned} \tag{5}$$

In Eq. (5), A represents the amplitude of the ac signal and ω is the (angular) frequency. A is chosen such that the contribution from the second term in the cosine coefficient is negligible and is small relative to the expected electron temperature, but not so small that the signal-to-noise ratio is within the experimental uncertainty in the measurement. The frequency of the ac signal must also be higher than the frequency of the dc probe sweep to obtain reasonable resolution for the second derivative. It should be kept lower than one tenth of the plasma frequency to prevent distortion in the EEDF [26]. The ac signal frequency must also be kept low enough to prevent the RC time constant of the measurement circuit from affecting the response by suppressing the ac signal. A full derivation of

this method can be found in Swift [31]. For this experiment a 2 V, 1 kHz ac signal was superimposed over the 10 Hz ramp voltage signal. To obtain the second derivative of the probe signal a lock-in amplifier is used to identify the signal corresponding to the second harmonic of the ac signal (the $\cos 2\omega t$term in Eq. (5)). The magnitude of this signal corresponds to the second derivative of the probe current with respect to voltage and is output directly from the lock-in amplifier (Stanford Research Systems SR810 DSP Lock-In Amplifier).

The plasma EEDF ($F(\varepsilon)$) can be represented by the product of the electron density (n_e) and normalized distribution function ($f(\varepsilon)$). The normalized distribution function takes the following form when the Druyvesteyn method is applied and a simplification of the electron energy distribution function adopted from Heidenreich [30].

$$f(\varepsilon) = \sqrt{\varepsilon}\,\frac{d^2I}{dV^2} \qquad \text{where } \varepsilon = \phi_p - V \tag{6}$$

The signal corresponding to the second derivative of the Langmuir probe trace produced by the lock-in amplifier cannot be used to directly calculate the normalized distribution function since the signal itself must be normalized. The following normalization constant was used to calculate the normalized EEDF.

$$H = \int_0^\infty \sqrt{\varepsilon}\,A(\varepsilon)d\varepsilon \tag{7}$$

Here *A* is the lock-in output. The lock-in output was used to generate a function proportional to the EEDF, which was normalized using the normalization constant.

$$f(\varepsilon) = \frac{\sqrt{\varepsilon}\,A(\varepsilon)}{H} \tag{8}$$

Equation (7) is used to normalize EEDF as calculated using the second derivative of the probe current generated by the lock-in amplifier, which is *A*.

D. Maxwellian Distribution with Velocity Shift

In the cathode plume, the neutral gas expands rapidly due to the low background pressure and the plume plasma transitions to a collisionless regime. The electrons are accelerated away from the keeper by the electric field provided by the anode potential. The anode in this case creates an electric field which is similar, conceptually, to that which would exist downstream of the cathode if it were operating with a thruster. Due to the large pressure gradient and strong electric field in the hollow cathode plume, the electrons are accelerated to a drift velocity higher than the local electron thermal velocity. This condition can lead to the formation of a double layer just downstream of the keeper exit, which is a well-established phenomenon in plasma physics and hollow cathode plumes [1]. A double layer can develop from several factors but in a hollow cathode it is formed due to the electron drift velocity exceeding the thermal velocity, or electrons having a Mach number greater than one. Downstream of the double layer, the plasma is collisionless; therefore, the accelerated electrons do not thermalize. Thus, a Maxwellian with a velocity shift can be observed in the cathode plume EEDF. Equation (9) describes a Maxwellian energy distribution function with a velocity shift in the z-direction, as derived by Shastry [32].

$$f(\varepsilon) = \left(\frac{1}{\pi k_b T_e \varepsilon_d}\right)^{1/2} \exp\left(-\frac{\varepsilon + \varepsilon_d}{k_b T_e}\right) \sinh\left[2\frac{(\varepsilon\varepsilon_d)^{1/2}}{k_b T_e}\right] \tag{9}$$

Here T_e is the electron temperature for the Maxwellian distribution and ε_d is the velocity shift expressed in terms of kinetic energy ($\varepsilon = 1/2\,mv^2$ and $\varepsilon_d = 1/2\,m(\Delta v)^2$), where, ε_d is considered a constant.

E. Collisional Cross Sections

The EEDF can be used to calculate reaction rate coefficients for known reactions in the plasma; however, this calculation requires knowledge of collisional cross sections associated with each reaction. For xenon, collisional cross sections are readily available in the literature and the plasma processes are very well known. For iodine, collisional processes are less well-known and cross sections for reactions are sparse, especially for vibrational excitations. To this end, an extensive literature search was conducted and relevant cross section data is summarized here and used for calculation of reaction rate coefficients for the cathode operating on iodine propellant.

Since iodine will dissociate at elevated temperatures (Moutinho [33] suggests that, for pressures at or below approximately $3 \cdot 10^{-2}$ torr, a large percentage of iodine vapor will be dissociated at temperatures above 1000 K), electron collisions with atomic iodine must also be considered in an iodine discharge generated in a hollow cathode. Equations (10), (11), (12) and (13) describe the reactions considered in the literature regarding a molecular discharge with iodine. These are not the only possible reactions for an iodine discharge; however, these were the only reactions with available corresponding cross section data.

Ali and Kim [34] used a binary-encounter-Bethe (BEB) model to calculate the electron-impact ionization cross sections of halogen atoms, diatomic halogen and hydrogen halide molecules, including atomic and molecular iodine. The calculated cross section for single ionization of atomic iodine for electron impact energies below 200 eV compares well with the experimental cross section reported by Hayes *et al* with an uncertainty of ±12% [35]. Hayes *et al* [35] also reported experimentally measured ionization cross sections for single, doubly and triply charged ions and the total ionization cross section for electron impact with atomic iodine from threshold to 200 eV. The total ionization cross section is the sum of the three ionization cross sections. Their results also agree well with theoretical results from Joshipura and Limbachiya [36] and Huo [37].

Ali and Kim [34] also calculate the ionization cross section for electron impact of molecule iodine resulting in a molecular ion. The cross sections are reported for electron energies from the ionization potential (9.31 eV) to approximately 5 keV. Here, no experimental data was available for comparison; however, the models of Ali and Kim [34] and Joshipura and Limbachiya [36] are in good agreement until the peak of the cross section. For energies beyond the peak, the model of Joshipura and Limbachiya [36] calculates a much larger cross section than Ali and Kim [34], suggesting an incorrect behavior at high energies. The peak cross section is located at electron energies of approximately 100 eV, which is much higher than is typically reported for hollow cathodes.

Prince *et al.* [38] report emission excitation cross sections for electron collisions with molecular iodine over an electron energy range of 4-100 eV. The cross sections are calculated from a collisional radiative model and experimentally measured spectra. The two excited states reported, identified by their respective transitions, are $B^3\Pi_{0+u}$ which relaxes to the ground state $X^1\Sigma_g^{-+}$ and $E^3\Pi_{0+g}$ which relaxes to the *B* state. Also identified by its transition is the molecular ion $A^2\Pi_{3/2u}$ which relaxes to the ground state.

Biondi and Fox [39] experimentally measured the absolute dissociative attachment cross section for electron impact with molecular iodine and compared their results with several other investigators, including Buchdual [40] and Healy [41]. Buchdahl used a total ionization tube method and Healy measured the attachment of a swarm of electrons directed through a gas by an applied electric field. The dissociative attachment cross section was determined for an electron energy range of 0.015 eV to 2 eV. Dissociative attachment is typically a low-energy process, with electron impact energies less than 10 eV, and is enhanced for atoms with high electron affinities. Typically, for atoms with high electron affinities, the electron capture is a resonant process.

The resonant capture process for iodine is described in detail by Frost and McDowell [42] and they reported a typical I^- capture peak, measured against a SF_6^- capture peak for comparison and experimental validation. The resonant capture process is reported from the onset energy (0.03±0.03 eV) to the upper energy limit (1.08±0.04 eV). The energy corresponding to the maximum capture cross section is 0.34±0.07 eV. In a later work describing ionization and dissociation, Frost and McDowell [43] describe how this resonant process influences negative ion production for electron impact with molecular iodine.

Tam and Wong [44] reported the cross sections negative ion current for the production of atomic halides from several halogen molecules including iodine. A unique feature in the iodine cross section is the rapid rise of negative ion current beginning at 9 eV, which is not seen in the cross sections of the other halides reported. It is postulated that the cause of this enhancement in the production of negative ions is caused by ion-pair formation [44]. This may have implications for the production of negative ions in the plume of a hollow cathode since this phenomenon spans the electron energy range on interest in hollow cathode discharges.

In more complex plasmas, such as ones including iodine molecules, many reaction products exist for collisions

Atomic Ionization	$e^- + I \rightarrow e^- + I^+$	(10)
Dissociative Attachment	$e^- + I_2 \rightarrow I^-$	(11)
Electronic Excitation	$e^- + I_2 \rightarrow e^- + I_2^*$	(12)
Molecular Ionization	$e^- + I_2 \rightarrow e^- + I_2^+$	(13)

involving electrons including vibrational excitation, electron attachment and dissociation. Knowledge of cross sections for specific reactions such as electron attachment, which is responsible for the formation of negative ions, is critical to understanding the dominant processes in the plasma. In typical plasma thrusters, negative ion formation is undesirable as electric fields are tailored to accelerate positive ions and accelerating negative ions into surfaces will increase degradation rates due to sputtering. In ion thrusters, negative ions effectively reduce the Bohm speed of ions entering the accelerating grids and reduce the beam yield [45]. Typically, electron attachment is most likely at low electron energies (<10 eV), which is exactly the electron energies typically found in electrostatic thrusters and hollow cathodes. Formation of negative ions will consume electrons, which would typically inhibit ionization; therefore, electron attachment is considered an efficiency loss at best and at worst it will quench the plasma and extinguish the discharge [46].

IV. Results

This section summarizes the plume characterization for the BaO MHC operating on xenon and iodine propellant. For this experiment the cathode was operated in triode mode (discharging to a flat plate anode), at the same discharge current, or anode current, for both propellants. Table 2 shows the steady-state cathode operating conditions for both propellants for the plume characterization. For operation on xenon, the iodine feed system was bypassed entirely to avoid contamination as would result if the cathode was operating on a mixture residual iodine and xenon of unknown concentration. The minimum xenon flow rate required for steady operation, i.e. maintaining a steady keeper potential, was 6 SCCM. The iodine pressure and temperature are consistent with a standard iodine vapor pressure curve.

Table 2. Cathode operating conditions for xenon and iodine propellants.

Propellant	V_K (V)	I_K (A)	V_A (V)	I_A (A)	T_{pot} (°C)	P_{pot} (torr)	Q (sccm)
Xenon	27	0.25	51	3.1	-	-	6
Iodine	30	0.25	65	3.1	52	8	-

A. Plasma Potential

Figure 5 shows the plasma potential time history as measured by a floating emissive probe for the nominal operating point listed in Table 2 for xenon. The mean plasma potential was 29.2 V with a RMS variation of 2.5 V. Figure 6 shows the power spectral density (PSD) estimate for the plasma potential. A slight hump is noticeable around 100 kHz; however, a sharp peak is clear at 10 kHz. The 10 kHz mode observed and shown in Figure 6 may be too low to be considered a result of ion acoustic oscillations which are typically in the 50 to 1000 kHz range and incoherent. Plasma potential fluctuations in this frequency range could be caused by ionization instabilities (50 to 250 kHz), which can be triggered by certain combinations of cathode operating conditions and geometry (i.e. orifice diameter, keeper-cathode orifice spacing, etc.).

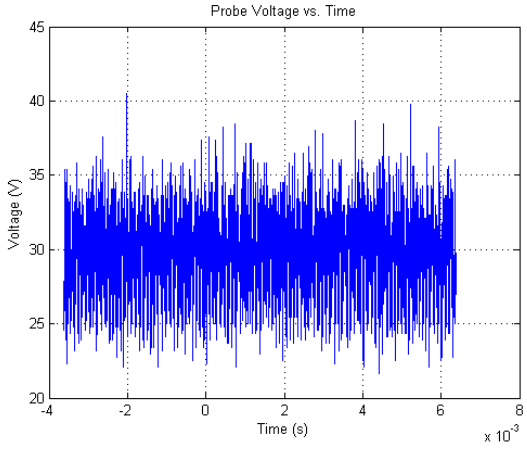

Figure 5. Emissive probe voltage (plasma potential) for the MHC operating on xenon.

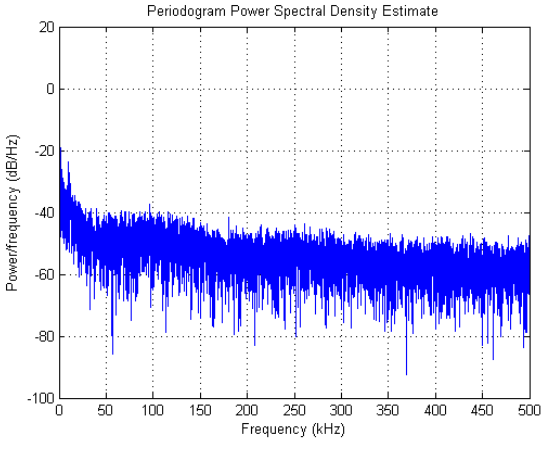

Figure 6. Power spectral density (PSD) of the plasma potential for the MHC operating on xenon.

Figure 7 shows the time history of the plasma potential for the BaO MHC operating on iodine at the nominal operating point listed in Table 2. For this case, the mean plasma potential was 43.7 V with a RMS variation of 0.76 V. The mean plasma potential is significantly higher with iodine than xenon (29.2 V). Figure 8 shows PSD for the plasma potential where some high frequency oscillations can be seen in the PSD, but they are quite low in amplitude. The strong, low frequency oscillations seen with xenon are not present with iodine; however a slight hump is noticeable at approximately 250 kHz, which is similar phenomenon observed with xenon.

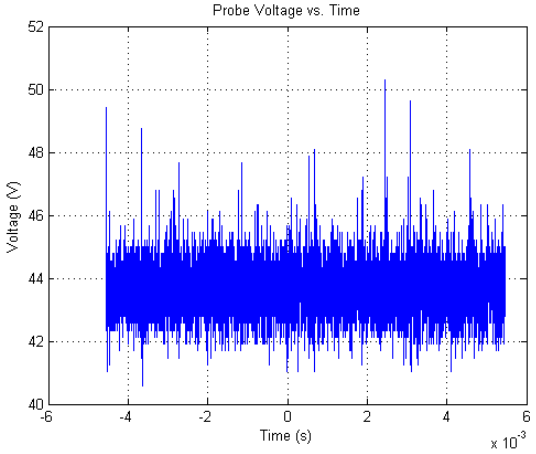

Figure 7. Emissive probe voltage (plasma potential) for MHC operating on iodine.

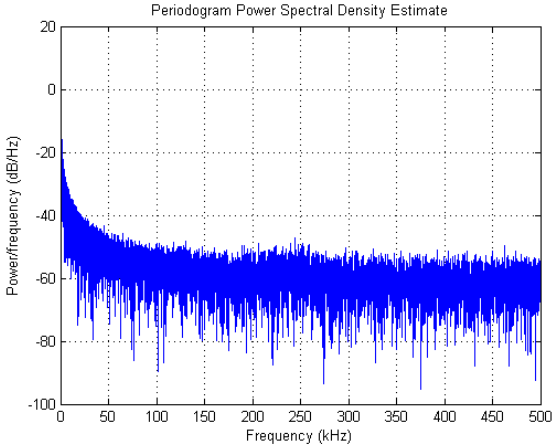

Figure 8. Power spectral density (PSD) of the plasma potential for the MHC operating on iodine.

B. Plasma Properties

To calculate the EEDF, the Druyvestyen method was used and the second derivative of the Langmuir probe current determined using the second harmonic method, as described in Section III. Figure 9 shows the measured EEDF in the near-keeper plume of the MHC operating on xenon. When the EEDF is known, the electron temperature can be obtained from the mean energy which can be determined by integrating the normalized EEDF. If the electron energy distribution follows a Maxwellian distribution, the electron temperature is proportional to the mean energy ($T_e = 2\langle\varepsilon\rangle/3$) and proportional to the difference between the floating potential and plasma potential ($T_e = 3.35(\phi_p - V_f)$). A simple check to determine if an EEDF follows a Maxwellian distribution is to calculate the electron temperature by integrating the measured EEDF and reproduce a Maxwellian distribution with the calculated electron temperature. The Maxwellian distribution shown in Figure 9 was calculated using the electron temperature from the integration of the measured, or Experimental, EEDF also shown in the figure. The measured distribution clearly deviates from a single temperature, Maxwellian distribution. Other distributions can exist in low temperature, low density plasmas with low ionization fractions similar to hollow cathode plume plasmas. Some distributions include the Druyvestyen distribution Bi-Maxwellian or "two-temperature" distribution, and Maxwellian distribution with velocity shift. Comparing the measured distribution with known variations of statistical distributions used to characterize electron populations, it was determined that the Maxwellian distribution with velocity shift best fit the measured EEDF. The Maxwellian distribution with velocity shift, expressed as a function of energy, was described in Section III, Part D. To fit a shifted

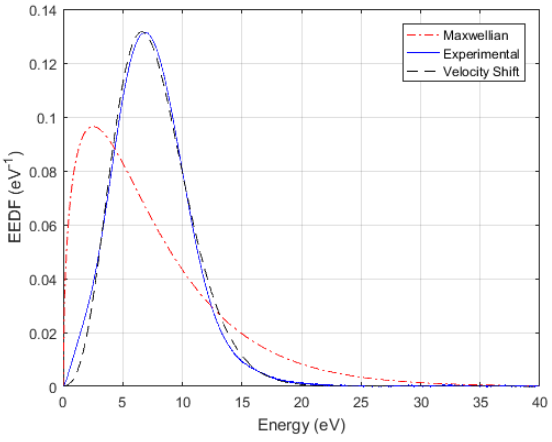

Figure 9. EEDF for MHC plume operating on xenon.

Maxwellian distribution to the measured EEDF, a MATLAB built-in function was used to optimize both the electron temperature (T_e) and velocity shift in terms of energy (ε_d) against the Experimental EEDF. The MATLAB curve fitting tool used a nonlinear least-squares algorithm to optimize the electron temperature and velocity shift.

Another method often employed to determine the electron temperature is a linear fit to the natural logarithm of the exponential region of the Langmuir probe curve after the ion contribution has been subtracted from the total probe current. For a Maxwellian distribution, the slope of the linear fit yields the electron temperature directly. Listed in Table 3 are electron temperatures calculated using several methods including the mean energy of the EEDF, linear fit to the exponential region of the Langmuir probe curve (often referred to as the slope method), relationship between the floating potential and plasma potential, and the fit to the experimental EEDF using the shifted Maxwellian distribution.

For both propellants, Table 3 lists the calculated electron temperatures using the three methods described above for a Maxwellian distribution; the mean electron energy, the slope method and difference between the plasma potential and floating potential. Table 3 also includes the electron temperature, velocity shift and electron Mach number for the Maxwellian distribution with velocity shift optimized to the measured EEDF Maxwellian distribution for both propellants. All of the electron properties listed in Table 3 were calculated using the measured EEDF. There is clear deviation for the electron temperatures calculated assuming a Maxwellian distribution. These temperatures are also much higher than the electron temperature for the Maxwellian distribution with velocity shift.

Table 3. Electron properties as calculated by several methods for each propellant.

Propellant	Electron Temperature by Method (eV)			Maxwellian with Velocity shift		
	Mean Energy	Slope Method	Floating Potential	T_e (eV)	ε_d (eV)	Mach No.
xenon	5.0	2.0	4.6	0.7	6.6	3.1
iodine	4.2	3.2	5.0	1.3	4.2	1.8

For xenon, the plasma density calculated using Orbit-Motion-Limited (OML) theory is $5.6 \cdot 10^{17}$ m^{-3}. Using the electron temperature from the integration of the EEDF the Debye length is $2.2 \cdot 10^{-5}$ m, which results in a probe-radius-to-Debye-length ratio of 1.72. This relationship between probe size and sheath thickness determines the applicability of the method used to determine the plasma density. OML theory accounts for a finite ion temperature, which implies that not all the ions that enter the sheath be collected by the probe. This requires a consideration of the ion angular momentum conservation and distribution function. OML theory is applicable for probe-to-sheath ratios of approximately 3 or less [47]. This ratio is too low for Thin Sheath theory to be applicable for any plasma parameter calculations, since this method is applicable for probe-to-sheath ratios of 10 or larger.

Table 4 lists calculated the reaction rate coefficients for several processes in a xenon plasma and includes the respective electron configuration. The reaction rates are calculated using the measured EEDF and cross section data [48]. The energy in parentheses for each excitation and ionization reaction corresponds to the threshold energy for that process.

Table 4. Reaction rate coefficients for the BaO cathode operating on xenon.

Process	$\langle \sigma v_e \rangle$ (m^3/sec)	Configuration	Type
$e^- + Xe \rightarrow e^- + Xe$	$4.44 \cdot 10^{-13}$	$\mathbf{5p^6}$	Elastic collision
$e^- + Xe \rightarrow e^- + Xe^*$ (8.315 eV)	$1.66 \cdot 10^{-14}$	$5p^5(^2\mathbf{P}^\circ_{3/2})6s$	Excitation
$e^- + Xe \rightarrow e^- + Xe^*$ (9.447 eV)	$1.83 \cdot 10^{-14}$	$5p^5(^2\mathbf{P}^\circ_{1/2})6s$	Excitation
$e^- + Xe \rightarrow e^- + Xe^*$ (9.917 eV)	$3.87 \cdot 10^{-14}$	$5p^5(^2\mathbf{P}^\circ_{3/2})5d$	Excitation
$e^- + Xe \rightarrow e^- + Xe^*$ (11.7 eV)	$1.68 \cdot 10^{-14}$	$5p^5(^2\mathbf{P}^\circ_{3/2})8d$	Excitation
$e^- + Xe \rightarrow e^- + Xe^+$ (12.13 eV)	$1.01 \cdot 10^{-13}$	$5p^5$	Ionization

Figure 10 shows the EEDF for the near-keeper plume region of the MHC operating on iodine. The EEDF is more similar to a Maxwellian distribution than the EEDF, in the same region, for the cathode operating on xenon. This could be due to a higher flow rate with iodine, resulting in a higher pressure and neutral density since it is difficult to precisely know the iodine flow rate. A higher pressure and neutral density may make it more likely for electrons to re-thermalize even in the presence of a double layer, or push the double layer further downstream and

beyond the interrogation area of the Langmuir probe. In either case, this would lead to a more Maxwellian-like distribution. Table 3 shows the electron temperature calculated from the measured EEDF using the mean electron energy, slope method and relationship between the floating potential and plasma potential for the cathode operating on iodine. Table 3 also lists the calculated electron temperature, velocity shift expressed as an energy and Mach number for the Maxwellian distribution optimized for the measured EEDF for the iodine plasma. Again, the electron temperatures calculated using the methods that assume a Maxwellian distribution clearly deviate from the electron temperature corresponding to the Maxwellian distribution with velocity shift.

For iodine, the plasma density calculated using OML theory is $6.8{\cdot}10^{17}$ m^{-3}. Using the electron temperature from the integration of the EEDF the Debye length is $1.9{\cdot}10^{-5}$ m, which results in a probe-radius-to-Debye-length ratio of 2.05. Again, this probe-to-sheath ratio is OML theory applicable, but is too low for Thin Sheath theory to be applicable.

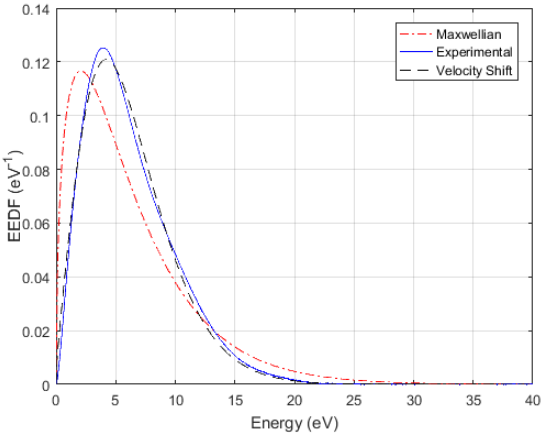

Figure 10. EEDF for MHC plume operating on iodine.

Table 5 lists the reaction rate coefficients for several processes in an iodine plasma. The reaction rates are calculated using the measured EEDF, calculated plasma density and cross section data from the iodine literature review. Since the cross sections for the iodine reactions could not be obtained from any database, plotted cross sections were digitized and interpolated in order to calculate the reaction rate coefficients.

Table 5. Reaction rate coefficients for the BaO cathode operating on iodine.

Process	$\langle \sigma v_e \rangle$ (m^3/sec)	Description
$e^- + I \rightarrow e^- + I^+$	$8.85{\cdot}10^{-14}$	Ionization from Ali [33]
$e^- + I \rightarrow e^- + I^+$	$9.63{\cdot}10^{-14}$	Ionization from Hayes [34]
$e^- + I_2 \rightarrow I^-$	$1.09{\cdot}10^{-16}$	Dissociative Attachment [38]
$e^- + I_2 \rightarrow e^- + I_2^*$ (E-B)	$2.59{\cdot}10^{-15}$	Excitation E-B [37]
$e^- + I_2 \rightarrow e^- + I_2^*$ (B-X)	$4.56{\cdot}10^{-16}$	Excitation B-X [37]
$e^- + I_2 \rightarrow e^- + I_2^+$	$1.85{\cdot}10^{-13}$	Molecular Ionization [37]

V. Discussion

A low power, BaO-W hollow cathode was operated on xenon and iodine propellants. Its performance, power consumption and plume properties were reported for xenon and iodine with the cathode at similar operating conditions for each. The overall performance of the BaO cathode on iodine was comparable to xenon, but the cathode required slightly higher power for ignition and discharge maintenance, as evident by the keeper voltage of 30 V (27 V for xenon) and an anode voltage of 65 V (51 V for xenon). Since the iodine flow rate could not be determined, the difference in operating power may have been due to a difference in operating conditions from xenon to iodine (i.e. higher flow rate with iodine). One reason may be related to equivalent mass and volumetric flow rates of xenon and iodine. Since iodine is a molecule, an equivalent mass flow rate of iodine can be achieved at roughly half of the volumetric flow rate of iodine. As a result, although iodine may not be fully dissociated at the cathode emitter there could be roughly half the number of candidates to ionize.

The ultimate cause of the higher required power is unknown; however, likely causes include kinetic processes associated with molecular plasmas. Two processes specific to molecular plasmas are rotational and vibrational excitation. These two processes are inelastic but do not provide a path to ionization in plasmas where excitation and ionization are driven by electron impact. Typically, in molecular plasmas, the number of low energy electrons is much lower when compared to an equivalent atomic plasma [49]. The reduction in the low energy population of electrons reflects the energy lost due to rotational and vibrational excitation. Therefore, the mean energy of electrons is smaller for molecular plasmas. At the same discharge current, the EEDFs for iodine show a lower mean

electron energy than with xenon (6.2 eV for iodine and 7.5 eV for xenon), which is consistent with molecular plasmas.

Another process specific to certain molecular plasmas is dissociative attachment. This process is specific to ions with an affinity to capture an electron forming a negative ion. Examples include, but are not limited to hydrogen (H_2), oxygen (O_2), sulfur hexafluoride (SF_6) and iodine (I_2) discharges. Dissociative attachment results in the generation of a neutral and negative ion. This could potentially be a significant electron loss mechanism since the product of the process does not include an electron. If low energy electrons are "disappearing" from the EEDF through the formation of negative ions, the remaining EEDF would shift to a higher mean energy. The significance of this reaction could be determined using the EEDF to calculate the reaction rate of this process; however, that would require knowledge of the dissociative attachment cross section and the number density according to species. Negative ions generated in the near plume of the discharge will "see" a relatively large potential hill towards the anode. If significant population of negative ions is generated by the cathode, this could have adverse effects on the operation and performance of a HET, possibly leading to accelerated channel erosion, and changes to the anode layer potential structure.

The measured EEDFs for both xenon and iodine propellants resemble a shifted Maxwellian distribution. When iodine is compared to xenon, the electron temperature is higher, but the energy corresponding to the shift is smaller in magnitude and relative to the respective electron temperature. This observation manifests itself in the calculated electron Mach number (3.1 for xenon and 1.8 for iodine). This may be a result of low energy electrons being consumed by low energy processes such as dissociative attachment. The shift in the distribution may be caused by several factors including electron acceleration through a double layer and/or electron streaming. For electrons being accelerated across a double layer in an iodine plasma the presence of negative ions will affect the double layer potential and effectively reduce the electron flux; thus, lowering the electron acceleration. For electron streaming, molecular processes could be inhibiting electron transport to the anode, effectively lowering the electron velocity. The reaction rate coefficient is small for the dissociative attachment process, but not small enough to be neglected entirely. Thus, negative ions may play a role in the operation of a cathode on iodine.

The reaction rate coefficient for ionization of atomic iodine is approximately an order of magnitude smaller than the reaction rate coefficient for ionization for xenon. Since it is likely that molecular iodine is mostly dissociated in the near plume region, ionization of atomic iodine may be the dominant reaction for ion generation. However, electron energy will be lost to the dissociation process, lowering the probability of ionization.

The reaction rate coefficients for the molecular processes are small but non-negligible, as with the dissociative attachment process. Since it is likely that most of the iodine has been dissociated by the near plume region, these values may be artificially inflated since this calculation assumes a plasma of 100% molecular iodine. Therefore, as these processes may play a role in lowering the effective electron energy their influence in the near plume region may be much reduced as compared to the insert plasma, where the degree of dissociation may be lower. Nevertheless, these processes will reduce the effective electron energy, lowering the probability of ionization.

Low frequency modes were not observed in the plasma potential measurements for iodine propellant, which were observed for xenon propellant. Coherent oscillations are commonly observed in the near plume of hollow cathodes operating on xenon propellant. The suppression of low frequency oscillations with iodine may be a result of higher neutral density (if the iodine flow rate is higher than xenon), lower mean electron energy and/or molecular processes. These processes may inhibit the growth of plasma waves and suppressing ion acoustic turbulence in the cathode plume.

VI. Conclusions

A BaO hollow cathode was operated on iodine propellant and the performance and plume characteristics compared to operation on xenon propellant. The hollow cathode operated stably on iodine, but at a higher operating power. This higher operating power, and parasitic power consumption by feed system heaters, etc. may be acceptable for many mission architectures. For such missions, single-propellant electrostatic propulsion systems using iodine may be attractive.

The ultimate source of the higher required power has yet to be determined, but it may be related to typical electron energy loss mechanisms associated with a molecular plasma (vibrational and rotational excitation, and dissociation). More research is required to quantify these mechanisms and determine their influence on the cathode discharge and required operating power.

The propensity exists for a hollow cathode operating on iodine propellant to generate negative ions. The results from this work show that it is plausible for a non-negligible population of negative ions to exist in the near-keeper region of the hollow cathode discharge. The true size of the negative ion population and the subsequent influence

on the operation of the hollow cathode, and further, the operation of a hollow cathode with an electrostatic thruster are unknown and merit further investigation.

For both propellants, the electron distribution appeared to follow a Maxwellian distribution with velocity shift. Electron drift velocities have been linked to the onset and maintenance of ion acoustic instabilities in the plume of hollow cathodes. The lower relative drift velocity for the cathode operating on iodine may indicate a higher plasma resistivity (or lower plasma conductance) between the cathode and anode.

References

[1] D. M. Goebel and I. Katz, Fundamentals of Electric Propulsion: Ion and Hall Thrusters, Hoboken: Wiley, 2008.

[2] M. Nakles, W. A. Hargus, J. Delgado and R. L. Corey, "A Performance Comparison of Xenon and Krypton Propellant on an SPT-100 Hall Thruster," in *International Electric Propulsion Conference*, Weisbaden, 2011.

[3] A. Shabshelowitz, A. D. Gallimore and P. Y. Peterson, "Performance of a Helicon Hall Thruster Operating with Xenon, Argon and Nitrogen," in *48th AIAA/ASME/SAE/ASEE Joint Propulsion Conference & Exhibit*, Atlanta, 2012.

[4] V. Hruby, B. Pote, T. Brogan, K. Hohman, J. Szabo and P. Rostler, "Air Breathing Electrically Powered Hall Effect Thruster". United States of America Patent US 6834492 B2, 28 December 2004.

[5] J. Szabo, M. Robin, J. Duggan and R. R. Hofer, "Light Metal Propellant Hall Thrusters," in *31st International Electric Propulsion Conference*, Ann Arbor, 2009.

[6] J. G. C. Szabo, V. Hruby and M. Robin, "Bismuth Hall Effect Thruster Development," in *JANNAF Propulsion Conference*, Monterey, 2005.

[7] J. Szabo, B. Pote, S. Paintal, M. Robin, G. Kolencik, A. Hillier, R. D. Branam and R. E. Huffman, "Performance Evaluation of an Iodine Vapor Hall Thruster," in *47th AIAA/ASME/SAE/ASEE Joint Propulsion Conference & Exhibit*, San Diego, 2011.

[8] O. S. Tverdokhlebov and A. V. Semenkin, "Iodine Propellant for Electric Propulsion--To Be or Not to Be," in *37th AIAA/ASME/SAE/ASEE Joint Propulsion Conference* , Salt Lake City, 2001.

[9] R. Dressler, Y.-H. Chiu and D. Levandier, "Propellant Alternatives for Ion and Hall Effects Thrusters," in *28th Aerospace Sciences Meeting & Exhibit*, Reno, 2000.

[10] S. George and N. Krishnamurthy, "Absorption spectrum of iodine vapor-An experiment," *American Journal of Physics*, vol. 57, no. 9, pp. 850-853, 1989.

[11] A. C. Hillier, R. D. Branam, R. E. Huffman, J. Szabo and S. Paintal, "High Thrust Density Propellant in Hall Thrusters," in *49th AIAA Aerospace Sciences Meeting including the New Horizons Forum and Aerospace Exposition*, Orlando, 2011.

[12] J. Szabo and M. Robin, "Plasma Species Measurements in the Plume of an Iodine Fueled Hall Thruster," *Journal of Porpulsion and Power*, vol. 30, no. 5, pp. 1357-1367, 2014.

[13] J. R. Wertz and W. J. Larson, Space Mission Analysis and Design, 3rd ed., Hawthorne: Microcosm Press, 1999.

[14] L. P. Rand and J. D. Williams, "Instant Start Electride Hollow Cathode," in *33rd International Electrical Propulsion Conference* , Washington D.C., 2013.

[15] K. M. Alexander and F. Fairbrother, "The Halides of Columbium (Niobium) and Tantalum. Part II. The Vapor Pressure of Tantalum Pentaiodide," *Journal of the Chemical Society*, pp. 2472-2476, 1949.

[16] H. Kamhawi, T. Haag, G. Benavides, T. Hickman, T. Smith, G. William, J. Myers, K. Polzin, J. Dankanich, L. Byrne, J. Szabo and L. Lee, "Overview of Iodine Propellant Hall Thruster Development Activities at NASA Glenn Reseach Center," in *52nd AIAA/SAE/ASEE Joint Propulsion Conference*, Salt Lake City, 2016.

[17] K. Polzin, S. Peeple, A. Burt, A. Martin, A. Martinez, J. Seixal and S. Mauro, "Development, Demonstration, and Analysis of an Integrated Iodine Hall Thruster Feed System," in *52nd AIAA/SAE/ASEE Joint Propulsion Conference*, Salt Lake City, 2016.

[18] J. W. Dankanich, M. Shelby, K. A. Polzin, H. Kamhawi, T. Hickman and Byrne, "The iodine satellite (iSat) Project Development towards Critical Design Review (CDR)," in *52nd AIAA/SAE/ASEE Joint Propulsion Conference*, Salt Lake City, 2016.

[19] R. F. Kemp and J. M. Sellen, "Plasma Potential Measurements by Electron Emissive Probes," *Review of Scientific Instruments,* vol. 37, p. 455, 1966.

[20] J. P. Sheehan, Y. Raitses, N. Hershkowitz, I. Kaganovich and N. J. Fisch, "A comparison of emissive probe techniques for electric potential measurements in a complex plasma," *Physics of Plasmas,* vol. 18, no. 7, pp. 1-9, 2011.

[21] V. A. Rozhansky and L. D. Tsendin, Transport Phenomena in Partially Ionized Plasma, London, New York: Taylor and Francis, 2001, p. 469.

[22] K. U. Riemann, "Plasma-sheath transition in the kinetic Tonks-Langmuir model," *Physics of Plasmas,* vol. 13, no. 6, pp. 1-13, 2006.

[23] F. Chen, "Electric Probes," in *Plasma Diagnostic Techniques*, New York, Academic Press, 1965, pp. 113-200.

[24] G. D. Hobbs and J. A. Wesson, "Heat flow through a Langmuir sheath in the presence of electron emission," *Plasma Physics,* vol. 9, no. 1, 1967.

[25] M. J. Druyvesteyn, "Der Niedervoltbogen," *Zeitschrift fur Physik,* pp. 781-797, 1930.

[26] Z. C. Lu, J. E. Foster, T. G. Snodgrass, J. H. Booske and A. E. Wendt, "Measurement of electron energy distribution function in an argon/copper plasma for ionized physical vapor deposition," *Journal of Vacuum Science and Technology A: Vacuum, Surfaces and Films,* vol. 17, no. 3, p. 840, 1999.

[27] H. W. Rundle, D. R. Clark and J. M. Deckers, "Electron Energy Distribution Functions in an O2 Glow Discharge," *Canadian Journal of Physics,* vol. 51, p. 144, 1973.

[28] K. F. Schoenberg, "Electron distribution function measurement by harmonically driven electrostatic probes," *Review of Scientific Instruments,* vol. 51, no. 9, p. 1159, 1980.

[29] S. W. Rayment and N. D. Twiddy, "Time-resolved measurements of electron energy distributions," *British Journal of Applied Physics,* vol. 2, no. 2, p. 1747, 1969.

[30] J. E. Heidenreich III, J. R. Paraszczak, M. Moisan and G. Sauve, "Electron energy distributions in oxygen mircowave plasmas," *Journal of Vacuum Science and Technology B,* vol. 6, no. 1, p. 288, 1988.

[31] J. D. Swift and M. J. R. Schwar, Electric Probes for Plasma Diagnostics, London: Iliffe Books Ltd, 1970.

[32] R. Shastry, A. D. Gallimore and R. R. Hofer, "Near-Wall Plasma Characterization of a 6-kW Hall Thruster," in *31st International Electric Propulsion Conference*, Ann Arbor, 2009.

[33] A. Moutinho, J. Aten and J. Los, "Temperature dependence of the total cross section for chemi-ionization in ackali halide-galogen collisions," *Physica,* vol. 53, pp. 471-492, 1971.

[34] M. A. Ali and Y.-K. Kim, "Ionization cross sections by electron impact on halogen atoms, diatomic halogen and hydrogen halide molecules," *Journal of Physics B: Atomic, Molecular and Optical Physcis,* vol. 41, no. 14, pp. 1-12, 2008.

[35] T. R. W. R. C. Hayes and R. S. Freund, "Absolute electron-impact-ionization cross section measurements of the halogen atoms," *Phys. Rev. A,* vol. 35, no. 2, p. 578, 1987.

[36] K. N. Joshipura and C. G. Limbachiya, "heoretical total ionization cross-sections for electron impact on atomic and molecular halogens," *International Journal of Mass Spectrometry,* vol. 216, no. 3, pp. 239-247, 2002.

[37] W. Huo, "NASA website," [Online]. Available: http://www.ipt.arc.nasa.gov/databasemenu.html.

[38] B. D. Prince, R. J. Bemish and D. J. Levandier, "Application of a First Generation Collisional Radiative Model for Iodine to Optical Emissions from the Plume of an Iodine Hall Effect Thruster," in *53rd AIAA/SAE/ASEE Joint Propulsion Conference*, Atlanta, 2017.

[39] M. A. Biondi and R. E. Fox, "Dissociative Attachment of Electrons in Iodine. III. Discussion," *Physical Review,* vol. 109, no. 6, pp. 2012-2014, 1958.

[40] R. Buchdahl, "Negative Ion Formation in Iodine Vapor by Electron Impacts," *Journal of Chemical Physics,* vol. 9, no. 2, pp. 146-152, 1941.

[41] R. H. Healey, "The behavior of electrons in iodine vapoir," *Philosophical Magazine and Journal of Science,* vol. 26, no. 179, pp. 940-953, 1938.

[42] D. C. Frost and C. A. McDowell, "Formation of I- Ion from I2 by Resonance Capture," *Journal of Chemical Physics,* vol. 29, no. 4, pp. 964-965, 1958.

[43] D. C. Frost and C. A. McDowell, "The Ionization and Dissociation of some Halogen Molecules by Electron

Impact," *Canadian Journal of Chemistry,* vol. 38, pp. 407-420, 1960.

[44] W.-C. Tam and S. F. Wong, "Dissociative attachment of halogen molecules by 0-8 eV electrons," *Journal of Chemical Physics*, vol. 68, no. 12, pp. 5626-5630, 1978.

[45] J. S. Snyder, "Investigation of the Feasibility of Fullerene Propellant for Ion Thrusters," NASA Technical Report, Jet Propulsion Laboratory, 1998.

[46] J. R. Anderson and D. Fitzgerald, "Design and Testing of a Fullerene RF Ion Engine," *AIAA-95-2664,* 1995.

[47] R. B. Lobbia and B. E. Beal, "Recommended Practice for Use of Langmuir Probes in Electric Propulsion Testing," *Journal of Propulsion and Power,* vol. 33, no. 3, pp. 566-581, 2017.

[48] "Biagi-v 7.1 (Magboltz version 7.1) database," [Online]. Available: http://www.lxcat.net. [Accessed 15 April 2015].

[49] M. Capitelli, M. Dilonardo and C. Gorse, "Coupled solutions of the collisional Boltzmann equation for electrons and the heavy particle master equation in nitrogen," *Chemical Physics,* vol. 56, pp. 29-42, 1981.

[50] S. 6. NIST Chemistry WebBook, "U.S. Department of Commerce," [Online]. Available: http://webbook.nist.gov/chemistry/.